Detection of progesterone in aqueous samples by molecularly imprinted photonic polymers

Sally Qasim[1] · Shu-Yu Hsu[2] · Ezequiel Rossi[3,4] · Zahra Salahshoor[1] · Chung-Ho Lin[2] · Luis Polo Parada[5] · Maria Fidalgo[1]

Abstract

A label-free molecular imprinted polymer (MIP) sensor was fabricated for the detection of progesterone in aqueous solutions, by polymerization inside the void spaces of colloidal crystals, which gave them photonic properties. The prepolymerization mixture was prepared from acrylic acid as the functional monomer, ethylene glycol as the cross-linker agent, ethanol as solvent, and progesterone as the imprinted template. After polymerization, the colloidal crystal was removed by acid etching and the target eluted with a solvent. Material characterization included as follows: attenuated total reflectance-Fourier-transform infrared spectroscopy, dynamic light scattering, swelling experiments, and environmental scanning electron microscopy. MIPs were investigated by equilibrium binding, kinetics experiments, and UV–visible spectra to investigate Bragg diffraction peak shift that occurs with the rebinding at different progesterone concentrations in deionized water and 150-mM NaCl solutions. The MIP response was investigated with progesterone concentration in the 1–100 μg L^{-1} range, with LOD of 0.5 μg L^{-1}, reaching the detected range of hormone in natural waters. Furthermore, hydrogel MIP films were successfully tested in various real water matrices with satisfactory results. Moreover, the MIP film exhibited good selectivity toward the progesterone hormone evidenced by a larger response than when exposed to structurally similar molecules. Computational studies suggested that size along with surface potential influenced the binding of analog compounds. Due to their ease of use and low cost, the sensors are promising as screening tools for the presence of progesterone in aqueous samples.

Keywords Molecularly imprinted polymer · Progesterone · Colloidal crystal · Photonic films · Bragg diffraction · Recognition ability

Introduction

Progesterone is a naturally occurring estrogenic compound in the cholesterol-long biosynthetic pathway. The average level of progesterone produced by women daily during their monthly cycle is about 20–25 mg and increases to 300–400 mg daily during pregnancy [1]. In addition, synthetic progesterone has been extensively used in human and veterinary therapies as growth promoters in cattle [2], as contraceptive pills, to promote regular menstrual cycles, to treat abnormal uterine bleeding, to control the symptoms of menopause, and to prevent endometrial cancer [3]. Large amounts of steroid hormones, as for example progesterone, testosterone, and estradiol, are released into surface waters, causing adverse biological effects both on humans and wildlife; commonly large quantities of progestonic entities are excreted through urine. The primary cause of the occurrence of progesterone and other endocrine disrupting chemicals

✉ Maria Fidalgo
fidalgom@missouri.edu

[1] Department of Civil and Environmental Engineering, University of Missouri, Columbia, MO 65211, USA

[2] Center for Agroforestry, School of Natural Resources, University of Missouri, Columbia, MO 65211, USA

[3] Dpto. de Ingeniería Química, Instituto Tecnológico de Buenos Aires (ITBA), CP1437, Buenos Aires, Argentina

[4] Consejo Nacional de Investigaciones Científicas Y Técnicas (CONICET), Buenos Aires, Argentina

[5] Department of Medical Pharmacology & Physiology, Dalton Cardiovascular Research Center, University of Missouri, Columbia, MO 65211, USA

in the environment is the release of untreated or partially treated effluents from the wastewater plants (WWTPs) [4]. Concentrations reported in surface waters ranged from 5 to 199 ng $L^{-}1$, and over 6300 ng L^{-1} in waste stabilization ponds (WSPs) [5].

High performance liquid chromatography (HPLC) with variety of detectors including ultraviolet–visible (UV–visible), diode array, fluorescence, and mass spectroscopy allows for the measurement of progesterone down to 0.04–2.01 ng L^{-1} in environmental waters, 0.08–2.84 ng g^{-1} in soils, 26–175 ng g^{-1} in sewage sludge, and 140–410 ng L^{-1} in wastewater [6]. Other methods have also been applied, combining adsorption or concentration media and analytical techniques: LC mass spectroscopy (LC–MS) [7], HPLC with diode-array detection (HPLC–DAD) [6]. Some of these methods require significant pretreatment steps, expensive, time consuming, and not easily accessible. Consequently, there is a need for simple and reliable method for the analysis of progesterone that will facilitate the detection and monitoring of this hormone in natural waters [8].

Molecularly imprinted polymer (MIP) fabrication process includes the spatial allocation of the target molecules via a careful design polymerization and creating a complementary binding nanocavities, a subsequent target removal and allowing the "key-lock" principle similar to enzymes rebinding mechanism, with high affinity to the target molecules [9]. MIPs have been reported for the detection of hormones and other endocrine disrupting chemicals in water [10], molecular imprinting-based solid-phase extraction (MI-SPE) has provided a powerful way to improve the recognition selectivity and detection sensitivity for chemo/bioanalysis in complex matrices [11], hydrophilic molecularly imprinted nanospheres (MINs) utilized as dispersant sorbent in matrix solid phase dispersion (MSPD) for the extraction of rhodamine B (RhB) as the illogical food additive dye from different foodstuffs, followed by HPLC analysis [12], and a specific recognition and extraction of the blood pressure regulating drugs valsartan (VAL) and losartan (LOS) using water compatible hollow porous molecularly imprinted nanospheres (HP-MINs) [13]. The high sensitivity and selectivity has been achieved applying a combination of diverse nanomaterials, sophisticated, complex sensing, and manufacturing processes. Photonic MIPs are label free sensors that combine non-covalent imprinting and colloidal crystal used as templates to produce optically active thin films [14]. Their simple operation makes them ideal candidates for field measurements or for point of care biomedical applications. However, their optical properties have shown to be very sensitive to the fabrication parameters, which resulted in variability between manufacturing batches. An enhanced control in the multi-step fabrication process and a full understanding of the effect of the parameters involved are highly needed but still lacking.

The objective of this work was to fabricate a photonic molecularly imprinted sensor for the detection of progesterone in aqueous media and to optimize the control in the fabrication processes by a systematically investigation of selected factors in the colloidal crystal formation, polymerization reaction, etching, and the target elution processes, mainly temperature, humidity, and colloid concentration during crystal growth, polymerization and acid bath time, and elution solution formulation in order to enhance both the morphological and chemical binding properties of the MIP.

We fabricated and tested a MIP capable of selectively recognizing progesterone in water samples. The label free-photonic MIP displayed shifts of the peak wavelength (λ_{max}) of their reflectance spectra driven by the selective rebinding of the progesterone molecules [15, 16]. The capture and detection of progesterone in test samples were investigated via equilibrium and kinetics tests. Subsequently, the effect of potential background interference, such as presence of dissolved salts and their selectivity in the presence of other steroid hormones with the similar chemical structure, was evaluated, through experiments and computational methods.

Methods and materials

Materials

Monodispersed silica particles with a diameter of 300 nm were obtained from Pinfire — Gems & Colloids (Frankfurt, Germany) and characterized by electron microscopy in a FEI Quanta 600 FEG Environmental Scanning Electron Microscopy (Thermo Fisher Scientific, Hillsboro, OR, USA) (https://www.thermofisher.com/us/en/home.html). Ethanol (99.5%, 200 proof), acrylic acid (AA) (99%), ethylene glycol dimethacrylate (EGDMA) (98%), methanol (99%), HPLC-grade progesterone standard, and 2,2'-azobisisobutyronitrile (AIBN) (98%) were purchased from Sigma-Aldrich (St. Louis, MO, USA) (https://www.sigmaaldrich.com/united-states.html). Progesterone (PG) (98%) was purchased from Cayman Chemical (Ann Arbor, MI, USA) (https://www.caymanchem.com) and used in the MIP fabrication process. Hydrofluoric acid (HF) (49%) and acetic acid (HAc) (96%) were supplied by Fisher (Fair Lawn, NJ, USA) (https://www.fishersci.com). A Thermo Scientific™ Barnstead™ E-Pure™ Ultrapure Water Purification System (Waltham, MA, USA) was used to high purity (type I) water (18.2 MΩ cm at 25 °C). All chemicals were reagent grade and used as received without further purification.

MIP fabrication

The sensor fabrication process involved the deposition of silica nanoparticles to form colloidal crystals, the infiltration

of the crystal structure by the pre-polymerization solution, polymerization, SiO_2 removal by HF, and elution of the target with a solvent (Fig. 1). A 1.3% volume fraction suspension of SiO_2 in ethanol was prepared, stirred at 600 rpm for 1 h and then sonicated for another hour. This process was repeated three more times. Clean glass slides were inserted vertically into the suspension and removed by a step motor in a custom-made chamber that allows for the control of the slide removal velocity and temperature during the deposition (Fig. 1a). The step motor was operated at a constant speed of 0.14 mm/min and the temperature was maintained at 70 ± 0.1 °C with a heated plated, controlled by an OMEGA a proportional–integral–derivative controller (PID) temperature controller CND3 series (Fig. 1b).

The pre-polymerization solution was fabricated as follows: 62.9 mg of PG was dissolved in 1 mL ethanol and AA (439 µl) was added; the mixture was left for 12 h at 4 °C to allow the complexation of the target with monomer via hydrogen bonding to proceed before addition of 302 µl of the crosslinker EGDMA, resulting in a molar ratio of 1:32:8 (PG:AA:EGMDA). Finally, 12 mg of AIBN was added as initiator. The optimum template-functional monomer-crosslinker molar ratio was chosen based on results from our previous studies; minimum resistance was provided using AA, it showed high penetration of the solution and diffusion of the target due to its hydrophilicity, while the polymer was cross-linked to a degree that it produced a connected matrix but still allowed some flexibility for the chains to swell/shrink upon binding/eluting of the target [17, 18]. A PMMA slide was placed on each side of the glass slide and one end of this "sandwich"-type structure was allowed to contact the pre-polymerization solution and infiltrated the colloidal crystal by capillary forces (Fig. 1c). The assembly was irradiated with UV light at $\lambda = 365$ nm for the polymerization reaction to proceed for 3 h (Fig. 1d). The glass slides and SiO_2 particles were etched in 5% HF for 36 h, followed by extensive rinsing with deionized water (Fig. 1e). In the last step, the target was eluted by washing the polymeric film with a 1:9 (v:v) HAc:EtOH solution, with replacement of solution every 30 min for a total of 3 h, and final rinse with ethanol in order to remove the HAc residues from the slides (Fig. 1f). Non-imprinted polymeric (NIP) films were fabricated as controls following the same steps as MIPs except for the addition of PG. Further fabrication details are added to the supplementary information section.

Characterization

The colloidal crystals and polymeric films were imaged to investigate the particle or pore size and morphology by a FEI Quanta 600 FEG (Thermo Fisher Scientific, Hillsboro, OR, USA) Environmental Scanning Electron Microscopy (SEEM). Samples were attached to stubs with conductive carbon tape and sputter with a thin layer of gold (1.5–3.0 nm) using an Emitech K575x sputter coater (Quorum Technologies Ltd., Ashford, Kent, UK). The images were analyzed using ImageJ software version 1.50 (National Institutes of Health, NIH). At least 3 different images for over 300 particles were measured.

A Zetasizer Nano ZS instrument (Malvern Instruments) was used to investigate the silica particle size distribution in the suspension by dynamic light scattering (DLS). At least 3 suspensions of silica nanoparticles were prepared independently with a concentration of 10 mg/L.

Attenuated total reflectance-Fourier-transformed infrared spectroscopy (ATR-FT-IR) was used to investigate the chemical structure of the material, and the spectra of the polymeric films were collected using a Nicolet 4700 FT-IR

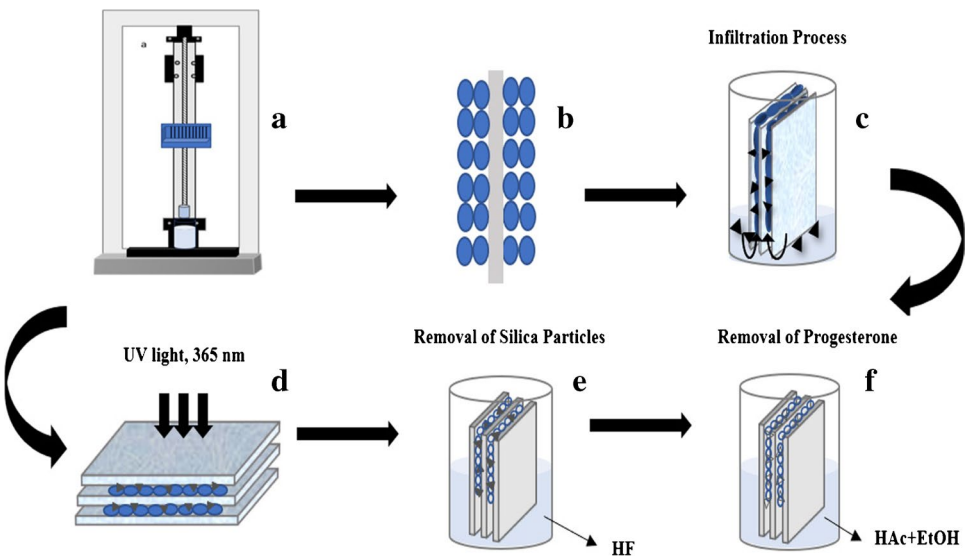

Fig. 1 Schematic representation of the MIP fabrication process: (**a**) silica deposition machine; (**b**) colloidal crystal formation; (**c**) infiltration process; (**d**) polymerization reaction; (**e**) silica particles etching; (**f**) target elution

(Thermo Electron Corporation, Waltham, MA, USA), between the wavelengths of 4000 and 400 cm^{-1}.

The equilibrium swelling experiments were performed on NIPs in phosphate buffer at two pHs (4 and 7), at 25 C. The polymers were swollen in solutions for 48 h at room temperature to reach equilibrium, and the degree of swelling was determined gravimetrically. The percentage of swelling ratio (SR) was evaluated from the following expression:

$$SR = \left(m_s - m_d\right)/m_d \quad (1)$$

where m_s is the mass of the swollen film at equilibrium and m_d the mass of the lyophilized films.

The optical response of the sensor was assessed by recording the reflectance spectrum before and after incubation in PG solutions, and the λ_{max} were connected with sample test concentration (see the Supplementary information).

In the kinetics experiments, the MIPs were first immersed in DI water for 20 min and then incubated under gently shaking in a 20 µg L^{-1} PG solution; slides were removed from the solution and reflectance spectra recorded every 2 min during at least 12 min. Equilibrium rebinding experiments were conducted in PG solutions of variable concentrations, from 1 to 100 µg L^{-1}. In a typical experiment, MIPs were first immersed in DI water for 12 min and then the films were incubated in 25 mL of each PG solution using a shaker (orbital shaker, Cole-Parmer, IL, USA) to facilitate the transport of the target molecule from the bulk solution into the porous film. After equilibrium was assumed, the slides were removed and rinsed with DI water and their reflectance spectra recorded.

The effect of ionic strength on the sensor response was investigated by the incubation in PG standard solutions with a background ionic strength of 150 mM as NaCl. This level of IS is representative of some industrial wastewater or brines, high salinity groundwater, or physiological conditions, as the sensor may be applied in the detection of PG in body fluids. To investigate the recognition ability of the MIP film and NIP film, a group of selected structurally similar compounds were selected: estradiol, hydrocortisone, and dehydroepiandrosterone-sulfate (Fig. S1 Supplementary data). The sensor response to a concentration 5 µg L^{-1} of the analog compounds was compared to that corresponding to PG. The measurements were repeated at least 5 times with different sensors for each hormone in the study. The concentration of all test solutions was validated by HPLC MS/MS. The analytical methods and the standard solutions preparation are in ESM (see the supplementary data).

The sensor was tested in real water samples collected from wetlands near Columbia, MO, and tap water at the University of Missouri (coming from Water Treatment Plant with Columbia Utilities) that were spiked with PG. Immediately after collection, the sampled water was characterized by pH, conductivity, and total organic carbon (TOC) measurements using a Shimadzu TOC-VCPN analyzer. The MIP sensor was first immersed in clean water for approximately 12 min and the initial diffraction peak measured; secondly, the sensors were dipped in the spiked solutions, let to equilibrate for 12 min, and rinsed with DI before reading wavelength shift. PG concentrations were determined by the optical response as established by the Bragg equation that relates the diffraction peak (λ_{max}) for the polymer. Sensor measurements were validated by analytical determinations of the PG concentrations in the samples, by liquid chromatography triple quadrupole mass spectrometry (LC–MS/MS). The experiments were conducted in triplicate.

Computational details

Calculations were performed using Gaussian 09 W software, applying the density functional theory (DFT) method with the hybrid Becke, three-parameter, Lee–Yang–Parr functional (B3LYP), and Pople's basis set 6-311G (2d,p) [19–21]. No symmetry constrain was imposed; potential energy surface minima were verified by vibrational frequencies [20]. Solvent effects were included using SMD continuum solvation model [20]. The molecular electrostatic potential mapped onto the isodensity surfaces was visualized using GaussView 6 [22] and the quantitative analysis of molecular surfaces were performed using Multiwfn 3.8 [23].

Results and discussion

Characterization of silica particles and films

The size of the silica particles was measured by DLS measurements. The results showed that the *Z*-average hydrodynamic diameter was 375 ± 7 nm, with a polydispersity index of 0.012. The results are in general good agreement with nominal values as reported by the manufacturer, since DLS commonly overestimates particle size due to the effect of the solvent on the hydrodynamic diameter.

Figure 2 shows the morphology of the colloidal crystals and the molecular imprinted polymeric films. Figure 2a and b show the top and cross-sectional view of the colloidal crystals structure. Particle size measurements from the SEM images yielded a size distribution of the particles, with an average radius of 232 ± 27 nm. Since the packing structure of a colloidal crystal is considered the crucial factor that determines its functioning in the optical application, the desirable thickness of the colloidal crystals film thickness was achieved by controlling the particle concentration in the suspension. A relationship was established between the thickness of the crystals and the volume fraction of particle suspension [24] as shown in Eq. 2:

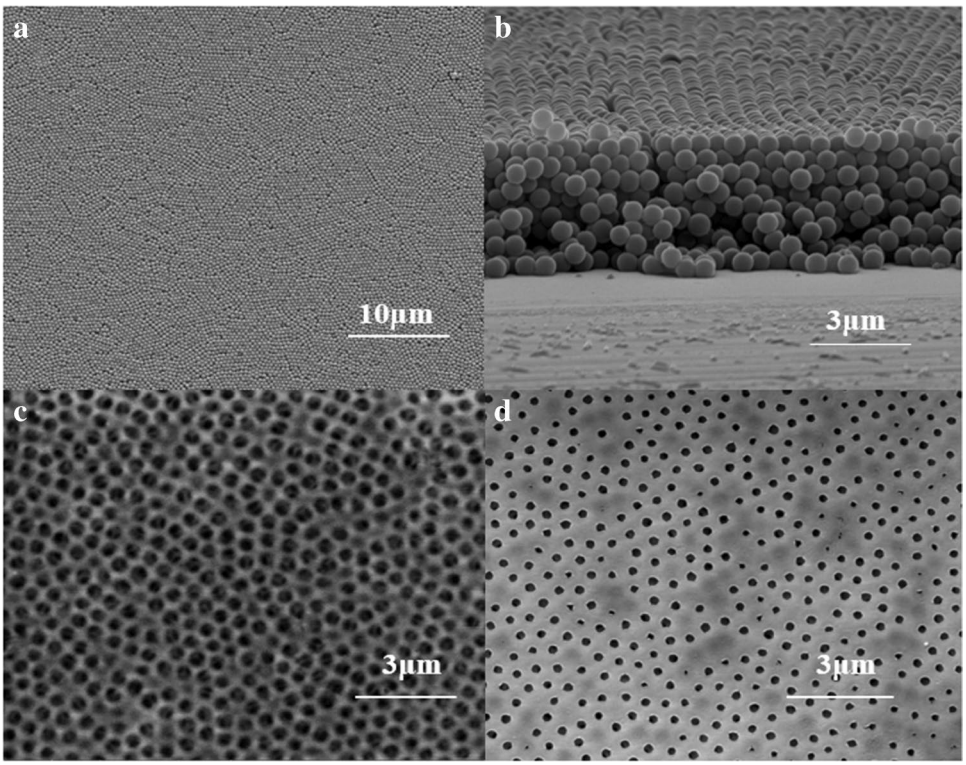

Fig. 2 SEM image of silica particles: (**a**) colloidal crystal top layer; (**b**) colloidal crystal cross section; (**c**) polymer structure; (**d**) surface porosity

$$K = \frac{\beta L \varnothing}{0.605 d(1-\varnothing)} \tag{2}$$

where K represents the number of layers, β is proportion of the particle velocity in solution to fluid velocity (assumed to be 1), L is meniscus height, d is the diameter of the particle, and $\varnothing$ is the particle volume fraction in the solution. The calculated number of layers according to Eq. 1, with $L\pm = 3500\ \mu m = 0.013$, $\beta = 1$, and $d = 232$ nm, was 328 layers. However, the number of layers observed in the SEM images was about 13–15 layers. Since Eq. 1 was derived for colloidal crystals fabricated by evaporation of ethanol at room temperature with a fixed vertical substrate [24], it is not unexpected that it did not provide a very accurate prediction their thickness under the conditions of the current study, as it overestimated the number of layers obtained. However, the inverse relationship between the particle volume fraction $\varnothing$ and the number of layers K was still valid. Figure 2c and d show the porous structure of the imprinted film after the removing of the silica. The surface porosity of the polymer afforded higher surface area and more available binding sites.

The bond between the chemical functional groups of the polymer and the PG molecule was investigated by ATR-FTIR. Spectra for MIP films before and after PG removal as well as NIPs were obtained (Fig. 3). Different absorption bands appeared for MIPs after PG removal compared to the MIPs before target removal and the NIPs. The ATR-FT-IR spectrum displayed a peak at 3000 cm^{-1} corresponding to O–H group, in the range 2500–3500 cm^{-1} of the characteristic profile of the carboxylic acids; this peak observed in the MIP film after target removal. Additionally, the peak at 1750 cm^{-1} is related to carbonyl group (C = O) of the monomer, which can be evidence of a total removal of the PG target from the MIP film. The non-covalent binding of the PG with the polymer before the washing process inhibited the absorption by the functional groups involved, while after PG removal, those groups were free to interact with the incident light and showed stronger adsorption bands [22].

The SR % of hydrogel film depends on the cross-linking and charge densities of the polymer network. High degree of the swelling translates into a larger variation in the photonic crystal structure, which, in turn, is associated with a more significant optical response. AA films presented high swelling ratio at neutral pH than at acidic pH (Fig. 4). At the higher pH, the carboxyl group is deprotonated to a higher extent, leading to electrostatic repulsion that causes the swelling ratio to be outweighed. On the other hand, at low pH value when carboxyl groups present in the polymer reduce the repulsive interactions between the polymer chains, resulting in less swelling, where AA expected to be present in its ionic form, with pKa of 4.26.

Analysis of manufacturing parameters

The colloidal crystal formation was investigated at 50 ± 0.1 and 70 ± 0.1 °C in order to investigate the effect

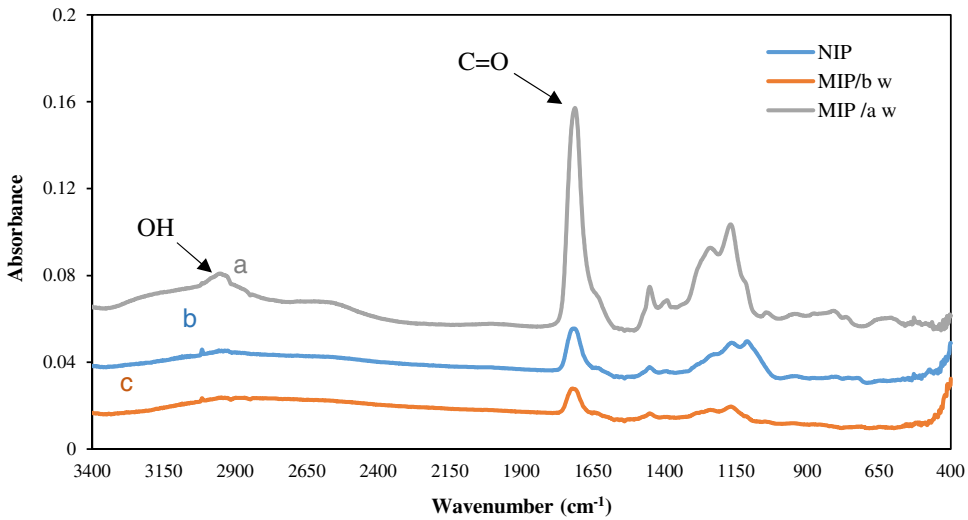

Fig. 3 ATR-FT-IR spectra of different films: (**a**) MIP after progesterone removal; (**b**) NIP; (**c**) MIP before progesterone removal

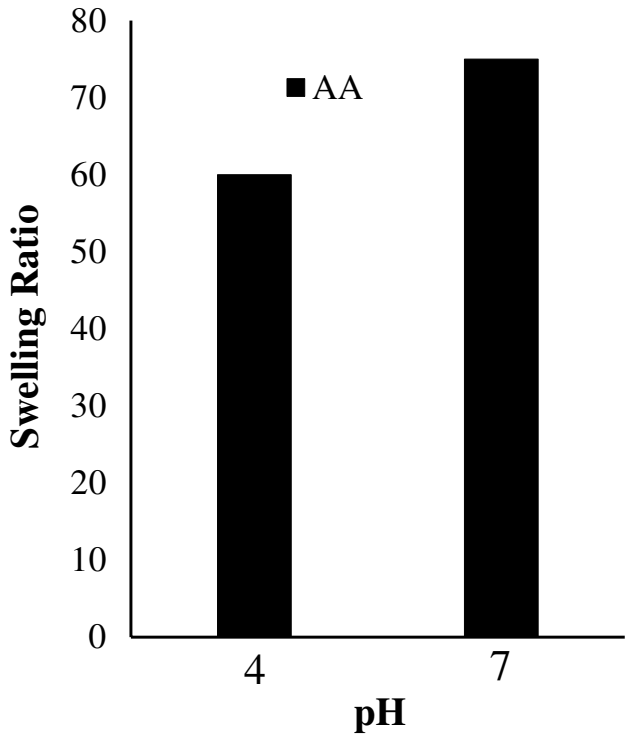

Fig. 4 Swelling ratio (%SR) variations of AA films with pH

of temperature on the uniformity and film thickness, and thus the diffraction properties of the opal films (see Fig. S2 in the supplementary data) [24]. However, the crystal deposition at temperature 70 °C was preferred for lower standard deviation values and the faster crystal formation.

Other variables were investigated in the photonic film fabrication: time in hydrofluoric acid bath, elution time, and solution concentration [25]. The 36-h time was superior to 24 h as it demonstrated higher shift values, evidencing better removal of silica particles without producing damage to the polymer film that was observed after 48-h immersion in the HF bath. In addition, three different washing ratios of acetic acid:ethanol (v:v) were considered for the PG removal. The results showed a maximum shift toward shorter wavelength of visible spectra region to an average of 395 ± 15 nm of the reflectance spectra with washing ratio (1:9) (Fig. S2c), which reflects the removal of the analyte from the binding sites and the shrinking of the hydrogel film [26]. Besides, the results showed that 3-h washing time had high efficiency of target molecule elution from the MIP matrix. Longer times proved to be excessive exposure to the acetic acid and ethanol solution, as the 4-h washing time caused damage to the film polymeric structure [1] and led to the shift back to higher wavelengths (Fig. S2d Supplementary data).

Kinetics and equilibrium of binding

The kinetics experiment of PG rebinding to the MIPs showed a progressive shift in the peak wavelength of the reflectance spectrum that leveled off after about 12 min, calculated as the average time of 6 different MIPs tested; the peak wavelength remained stable for the remainder of the experiment (Fig. S3, Supplementary materials). The adsorption of PG into the imprinted sites involves the transport of the molecule form the bulk of the solution to the binding site and the adsorption step. The porous morphology of the sensor is expected to provide numerous binding sites close to the polymer-liquid interface, which can be reached relatively fast, and other sites inside the polymer matrix. The utility of the latter for sensing is limited by the diffusion step of the molecules through the solid, which is much slower than the movement through the liquid in the pores. Gently mixing was applied during incubation in this work, to accelerate the transport of PG molecule through the porosity, leading to shorter equilibration times that those previously reported [17].

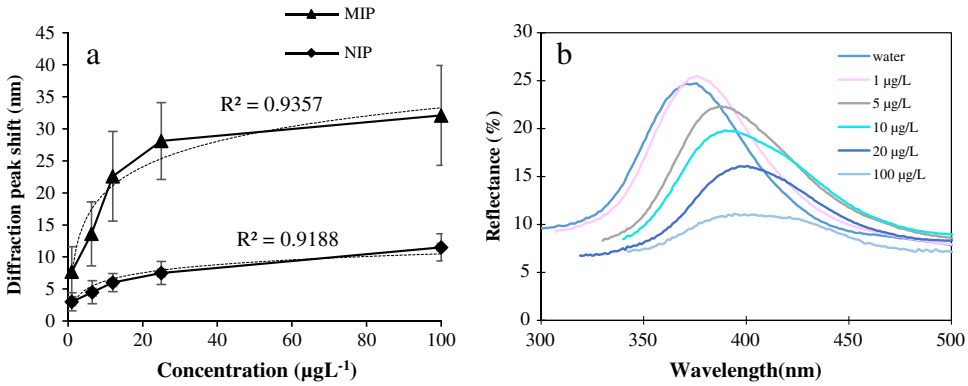

Fig. 5 Optical response of MIP sensors after incubation at various concentration of PG aqueous solutions: (**a**) diffraction peak shift; (**b**) reflectance spectra. The standard deviation and mean average are calculated based on the measurements of at least ten individual MIP sensors for each concentration (sample volume = 25 mL, incubation time = 12 min, temperature = 25 °C, $n = 10$)

The equilibrium incubation experiments showed a gradual shift to higher wavelengths in the peak of the reflection spectra with increasing concentration of PG solutions; the shift was measurable after exposures to concentrations as low as 1 μg L^{-1}. Ten MIP films were tested in each solution; the average and standard deviation of the observed shifts are shown in Fig. 5a. The photonic properties of the MIPs changed with the amount of the rebinding of PG molecules, which in turn can be correlated with the peak wavelength of the reflection spectrum; increasing the concentration of the target in the incubation solutions produced a shift of the peak to a longer wavelength [22–24]. Moreover, the shift observed after exposing the NIPs to the PG solutions was much lower, which revealed some degree of non-specific adsorption occurred in the NIP films, that can be interpreted as background or noise for the technique.

Figure 5b shows the result of the observed reflection spectra of the MIPs incubated in solutions of different concentrations of PG. A noticeable decrease in λ_{max} intensity appeared with increasing PG concentrations. This can be attributed to uneven swelling of the porous hydrogel during rebinding, producing an uneven deformation of the structure that reduced its photonic characteristics. However, peak wavelength values could be identified for each case, with no negative effect over the sensor performance.

The MIP sensor was able to detect concentrations of PG from 1 to 100 μg L^{-1} (Fig. 5). The detection limit (LOD) was determined to be 0.5 μg L^{-1}, and LOD was calculated as the concentration resulting from three times the standard deviation of 5 independent measurement of the blank (3σ criterion) (standard deviation measured on wavelength = 4.9 nm) (S/N = 3) [5].The limit of quantification (LOQ) was determined to be 2 μg L^{-1}; it was calculated as ten times the standard deviation of 5 independent measurement of the blank (10 σ criterion) (standard deviation measured on wavelength = 9.5 nm) (S/N = 10). The MIP exhibited relatively a linear response with concentration, between 1 and 20 μg L^{-1}, but flatten to a plateau as it approached saturation for higher concentrations. A larger total diffraction peak shift denoted a much stronger binding affinity of PG to the MIP than NIP.

The same manufacturing protocol was carefully followed in the fabrication of all MIP sensors. However, the high standard deviation of the measurement values in (Fig. 5a) evidenced variations in films, possibility due to differences in binding cavities in the polymeric structures and degradation or unreacted compounds that act as contaminants of solutions during sensor use. Generally, the affordability, ease of fabrication, and use make MIPs an ideal technology for on-site screening and/or quantification of PG in water. Although film reproducibility was improved by the analysis of parameter presented in this study, more work is needed in the control of the fabrication process that will enhanced the accuracy of the technology [27].

A comparison of the sensor developed in this work with others reported in the literature evidences its shortcomings. For example, MIP-based sensors for progesterone combined with surface plasmon resonance, gas chromatography-flame ionization, or HPCL achieved LODs of 8.8×10^{-12} ng/mL [28] and 1.1×10^{-4} ng/mL [10, 29] for the first, second, and third cases respectively. These values are much lower than the one reported in this work; however, a direct comparison with these methods ignores the pros of our proposed sensor. Optical and in particular photonic sensors have the advantage of being simpler, since they are label free and do not require complex analytical equipment to read their responses, which can be particularly important for in situ measurements.

Effect of ionic strength

The variation of sample characteristics (i.e., ionic strength) might affect the sensor response in the form of peak wavelength shift not associated with PG rebinding [30]. The ionic strength (IS) of the test solution may affect the sensor response in two main ways: first, the addition of charged ions would results in the compression of the electric double layer at the polymer-solution interface and a decrease in the electrostatic repulsive forces of the surfaces within the pore structure, which contribute to less swelling under similar

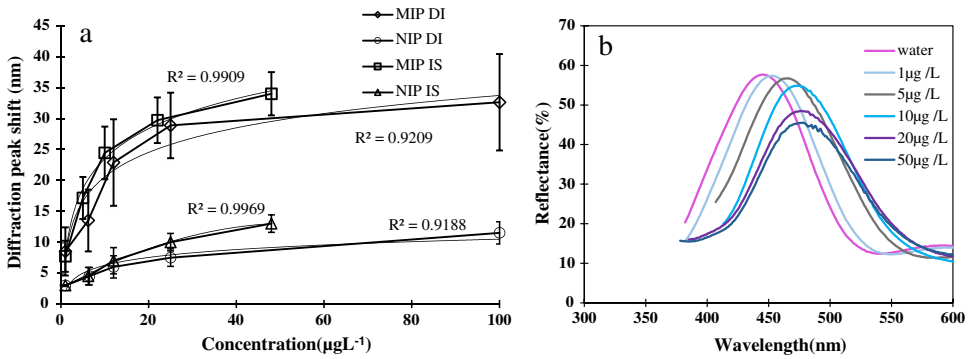

Fig. 6 Optical responses of the MIP sensors after incubation at various concentrations of PG aqueous solutions, 150 mM NaCl. The standard deviation and mean average are calculated based on the measurements of at least ten individual MIP sensors for each concentration: (**a**) diffraction peak shift; (**b**) reflectance spectra (sample volume = 25 mL, incubation time = 12 min, temperature = 25 °C, $n = 10$)

rebinding conditions; second, the influence of salt ions on the MIP binding affinity under the Hofmeister effect.

The MIPs were applied to the quantification of PG in standard aqueous solutions with a background ionic strength of 150-mM NaCl concentration (Fig. 6). While the average peak wavelength shift at each PG concentration was similar to the deionized water solutions, much less variability at 150 mM IS was observed in the readings of different sensors. The responses resulted in lower standard deviations, narrower peaks, higher reflectance intensity, and more consistent responses of the polymer hydrogel film other than for the deionized water solution.

The larger peak shift hints to an enhanced binding efficiency of the MIPs after incubation in IS solutions [24, 25, 31] with respect to that observed in deionized (DI) water solutions (Fig. 6a). This can be related to the effect of IS on the hydrogel swelling degree [32] as well as the increased non-specific adsorption and interaction with compounds promoted by the IS. This enhanced optical response of MIP IS with suggested that the second effect is more likely and pronounced than the first one in this case, which can be explained by the solvation energy disparities between the kosmotropic salt ions and the neighboring water molecules. The observation follows the mechanism of the Hofmeister series of cations, especially being the sodium the most kosmotropic cation [33]. The kosmotropic ion presence can increase of the general cohesiveness of the solution by the solvation energy, as well as the hydrogen bonding between PG and the polymer, thus decreasing the interference from the water molecules in the recognition nanocavities.

Effect of analog compounds

The selected analog compounds are steroid hormones, naturally synthetized from the cholesterol molecule and have chemical structures similar to PG. Other compounds can potentially be adsorbed into the imprinted cavities, if they have comparable molecular size and similar functional groups, and as a result hinder the correct determination of PG by the MIPs. Consequently, the binding affinity of the MIPs for PG might be affected significantly by the presence of the analog hormones, and the sensor optical response as well.

The binding affinity depends mainly on the size and shape of the target molecule, as well as the degree of interaction of binding sites. The target preferentially occupied the imprinted cavities within the hydrogel film due to the congruent shape, size, and interaction sites with the formed binding sites.

The PG MIPs were incubated in 5 μg L^{-1} solutions of each one of the chemicals and the results are shown in Fig. 7. As expected, the MIPs showed the highest response toward the PG hormone with a peak wavelength shift of 12 ± 3.5 nm due to the affinity of the PG to the imprinted nanocavities within the film. Incubation of the film in the 17-β estradiol solution produced a shift of 6 ± 2.5 nm, about half of the target molecule. Estradiol is the closest to PG in chemical structure of all tested compounds, slighter smaller with some differences in functional groups two hydroxyl groups in lieu of ketone groups. Hydrocortisone solutions yielded a shift of 4.7 ± 3.2 nm; although hydrocortisone shares many structural and functional groups characteristics with PG, the results suggested that the additional carbon in the C17 chain effectively decreased the binding affinity to the PG-imprinted sites. On the other hand, the DHEA-S test solution gave the lowest wavelength shift value with 2.7 ± 2 nm. The presence of the sulfate group attached from C3 appeared to produce a steric hindrance to the rebinding and lowered the binding affinity within the film. Meanwhile, a minimum response toward the adsorption solutions without specific binding cavities, and thus, one type of non-specific adsorption interaction showed by the NIPs, due to the general attraction between the polymer surface material and the compounds. The selectivity of NIPs was evaluated as an

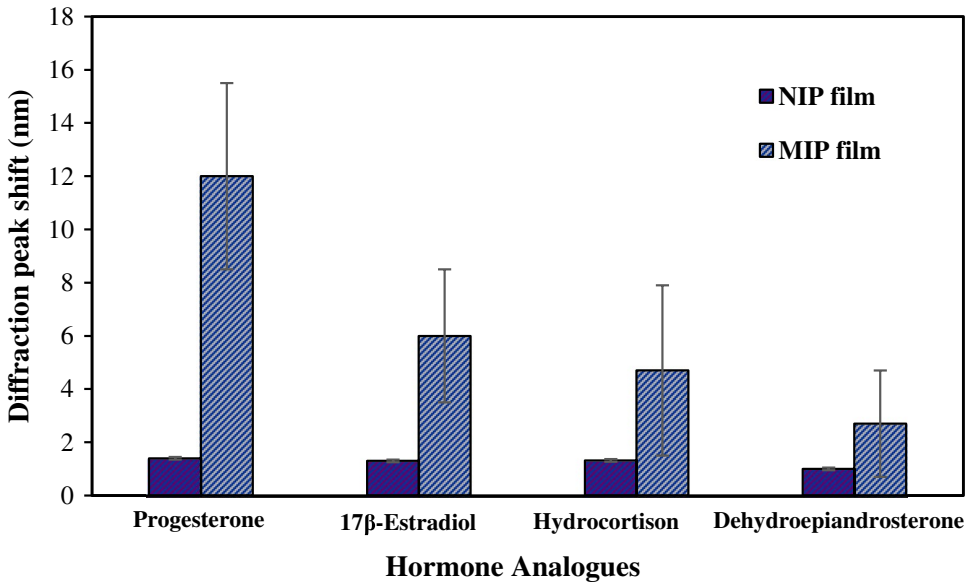

Fig. 7 The diffraction peak shift of the MIPs and NIPs when incubated in progesterone and 3 potential interfering compounds (17β-estradiol, hydrocortisone, dehydroepiandrosterone sulfate) (sample volume = 25 mL, incubation time = 12 min, solution concentration = 5 μg L^{-1}, temperature = 25 °C, $n = 5$)

average diffraction peak shift as 1.1, 1.3, 1.19, and 1.2 nm for progesterone, 17β-estradiol, hydrocortisone, and dehydroepiandrosterone sulfate, respectively.

Although the sensor response was significantly higher for PG than for the other molecules, the results indicated that a similar but smaller molecule may be able to bind to a significant degree and produce a false reading of PG concentration. The binding affinity of different analogs toward the MIP and NIP film revealed that the specific binding sites are the key for the recognition of the template molecule.

In order to compare the molecular shape, size, and electrostatic potential values of the selected hormones, the molecular electrostatic potential surface, which is a plot of electrostatic potential (ESP) mapped onto the iso-electron density surface, was calculated (see Fig. S3 Supplementary data) [34]. Regions with most negative and most positive electrostatic surface potentials are colored with red and blue, respectively. In addition, quantitative analyses were performed, and the calculated parameters are presented in Table S2 Supplementary data.

The only molecule that is smaller than progesterone is the estradiol, and, consequently, it the only one that can fit in all cavities imprinted by progesterone in MIP sensors (see table S2). This is because its aromatic ring that makes planar that part of the molecule, as it can be appreciate in the side-view in Fig. S3. Although its smaller size, the estradiol exhibited less interference that could be expected (Fig. 7); the observation can be explained comparing the ESP distribution on the iso-electron density surface and the polarity of the molecule. Estradiol surface is dominated by nonpolar interactions (62.3% of its area is nonpolar) and is the hormone with the smaller molecular polarity index. In addition, the top-view in Fig. S3 shows that the ESP distribution on both hormones is quite different. These factors make it difficult for estradiol to interact with the functional groups imprinted in the cavities by progesterone. On the other hand, hydrocortisone and DHEA-S have more similar ESP distribution on the iso-electron density surface and polarity. However, the volume of these hormones is larger than progesterone and therefore, they cannot fit in all cavities imprinted in MIP sensors. This is in agreement with the low interference by these molecules observed in the assays.

Analytical applications in natural water samples

In the composition of complex real natural water samples, there may be challenging components and characteristics, such as pH, dissolved solids, and natural organic compounds. To further test the applicability of the sensor, the MIP films were used for the determination of PG concentrations in two types of real waters: natural water samples obtained from creeks near Columbia, MO (Glendale Rd & Maupin Rd) and tap water from the laboratory at the University of Missouri. The collected samples were spiked with PG and its concentration measured by the newly fabricated sensor and compared to liquid chromatography triple quadrupole mass spectrometry (LCMS/MS), which were considered the true concentration values. The corresponding analysis results are listed in Table 1. Both the natural water and tap water had a neutral pH. The IS of the tap water was much higher than the natural water samples, and it was expected to have some effects on the sensor performance. The TOC level of the natural water was higher than tap water due to the existence of dissolved NOM.

The readings by the MIP sensor in tap water were closer to the true values than in natural water samples. The matrix complexity results in a higher chance of block the cavities or the surfaces of sensor films. Still, the values in both tap

Table 1 Measuring of PG in real water samples and their physicochemical characteristics

Sample	Sensor measured PG concentration (μg L^{-1})	Stdev	Error (%)	LC–MS/MS measured PG concentration (μgL^{-1})	pH	IS (mM)	TOC (ppm)
Glendale Rd	17.75	0.56	27.4	13.9	7.45	2.3184	4.287
	8.2	0.42	5.6	8.6			
Maupin Rd	20.1	0.35	17.1	24.2	7.13	1.016	2.212
	8.05	0.21	23.3	10.5			
Tap	19.4	0.78	17.1	23.0	7.2	13.8	N/D

and wetlands were reasonably close to the LCMSMS measured PG concentrations. The sensor underestimated the PG concentration in the high PG level natural water samples: the TOC content in in natural water and possible contributions of other unknown pollutants and particulate matter that can cause interference with the sensor performance may have affected the measurements, while tap water constitutes a much simpler and well-known matrix. IS did not show results in negative effects in the measurements, as demonstrated by the good readings obtained for the tap water samples. The MIP results revealed satisfactory recognition ability toward the analyte, and a promising performance in challenging, unknown natural water samples.

Conclusions

Molecularly imprinted polymeric films were fabricated with highly ordered 3D structures that conferred them photonic properties. Analysis of the manufacturing parameters showed that a temperature of 70 °C for the colloidal crystal fabrication, 36-h etching time, and a 1:9 (v/v) acetic acid:ethanol ratio for 3 h yielded the best results. High-quality colloidal crystals were obtained in a custom made equipment, and the following steps in the fabrication process are capable of automatization through a similar approach. This would not only result in higher throughput in manufacturing but also significant reduction in waste, minimizing chemical consumption and waste production, addressing one of the main drawbacks of MIP technology. However, variability still remained high, as evidenced by the error bars in the calibration curves, and more research is needed to improve the polymerization and target removal steps of the manufacturing process.

The sensors demonstrated high response after exposures to concentrations down to 1 μg L^{-1} and 12-min equilibrium time, with LOD 0.5 μgL^{-1}. Significant improvement in the response was observed by the incubation in standard aqueous solutions with a background 150 mM NaCl, with much less variability in sensor response and slightly higher wavelength shifts at each concentration tested. Moreover, the developed sensor was successfully applied to detect progesterone in the presence of complex matrices, in both natural water and tap water samples, with errors between 1 and 27%, which suggest the use of the sensor to quantify PG at low concentrations or as a screening tool for the presence of PG in natural water. Furthermore, higher affinity for PG in the presence of other steroid hormones (structural analogs) was illustrated the good recognition of the MIPs that proved via the computed surface electrostatic potentials and the ability to form bonds with the polymer functional groups. Appreciable advantage exhibited with higher specificity of MIP films over NIP films toward PG hormone with other structurally related analogs.

This work has shown the potential for photonic MIPs in environmental applications. The use of the sensor is straightforward and fast, while it is capable to differentiate hormones with similar structures to PG. Moreover, the sensor can find uses in biomedical applications, as for example blood analysis, where several hormones are expected to be present in the sample. However, hormone concentrations can vary widely and expected levels of each hormone concentration at any given time for one individual are rarely similar, which will impact possible interference effect. In those cases, background information about the sample, such as individual gender, age, and medical conditions, should be part of the interpretation of the sensor response.

Supplementary Information The online version contains supplementary material available at https://doi.org/10.1007/s00604-022-05290-w.

Declarations

Conflict of interest The authors declare no competing interests.

References

1. Ričanyová J, Gadzała-Kopciuch R, Reiffova K, Bazel Y, Buszewski B (2010) Molecularly imprinted adsorbents for preconcentration and isolation of progesterone and testosterone by solid

phase extraction combined with HPLC. Adsorption 16(4):473–483. https://doi.org/10.1007/s10450-010-9265-7
2. Fent K (2015) Progestins as endocrine disrupters in aquatic ecosystems: concentrations, effects and risk assessment. Environ Int 84:115–130. https://doi.org/10.1016/j.envint.2015.06.012
3. Golovko O, Šauer P, Fedorova G, Kroupová HK, Grabic R (2018) Determination of progestogens in surface and waste water using SPE extraction and LC-APCI/APPI-HRPS. Sci Total Environ 621:1066–1073. https://doi.org/10.1016/j.scitotenv.2017.10.120
4. Kumar V, Johnson AC, Trubiroha A, Tumová J, Ihara M, Grabic R, … Kroupová HK (2015) The challenge presented by progestins in ecotoxicological research: a critical review. Environ Sci Technol 49(5), 2625–2638https://doi.org/10.1021/es5051343
5. Kasambala HR, Rwiza MJ, Mdegela RH (2019) Levels and distribution of progesterone in receiving waters and wastewaters of a growing urban area. Water Sci Technol 80(6):1107–1117. https://doi.org/10.2166/wst.2019.350
6. Huang X, Yuan D, Huang B (2008) Determination of steroid sex hormones in urine matrix by stir bar sorptive extraction based on monolithic material and liquid chromatography with diode array detection. Talanta 75(1):172–177. https://doi.org/10.1016/j.talanta.2007.10.052
7. Tomšíková H, Aufartová J, Solich P, Nováková L, Sosa-Ferrera Z, Santana-Rodríguez JJ (2012) High-sensitivity analysis of female-steroid hormones in environmental samples. TrAC, Trends Anal Chem 34:35–58. https://doi.org/10.1016/j.trac.2011.11.008
8. Chang H, Wan Y, Wu S, Fan Z, Hu J (2011) Occurrence of androgens and progestogens in wastewater treatment plants and receiving river waters: comparison to estrogens. Water Res 45(2):732–740. https://doi.org/10.1016/j.watres.2010.08.046
9. Alvarez-Lorenzo C (2013) Handbook of molecularly imprinted polymers. Smithers Rapra
10. Cáceres C, Bravo C, Rivas B, Moczko E, Sáez P, García Y, Pereira E (2018) Molecularly imprinted polymers for the selective extraction of bisphenol A and progesterone from aqueous media. Polymers, 10(6). https://doi.org/10.3390/polym10060679
11. Arabi M, Ostovan A, Bagheri AR, Guo X, Wang L, Li J, … Chen L (2020) Strategies of molecular imprinting-based solid-phase extraction prior to chromatographic analysis. TrAC Trends Anal Chem 128, 115923https://doi.org/10.1016/j.trac.2020.115923
12. Arabi M, Ostovan A, Bagheri AR, Guo X, Li J, Ma J, Chen L (2020) Hydrophilic molecularly imprinted nanospheres for the extraction of rhodamine B followed by HPLC analysis: a green approach and hazardous waste elimination. Talanta 215:120933. https://doi.org/10.1016/j.talanta.2020.120933
13. Gholami H, Ghaedi M, Ostovan A, Arabi M, Bagheri AR (2019) Preparation of hollow porous molecularly imprinted and aluminum(III) doped silica nanospheres for extraction of the drugs valsartan and losartan prior to their quantitation by HPLC. Mikrochim Acta 186(11):702. https://doi.org/10.1007/s00604-019-3794-x
14. Casis N, Busatto C, Fidalgo de Cortalezzi MM, Ravaine S, Estenoz DA (2015) Molecularly imprinted hydrogels from colloidal crystals for the detection of progesterone. Polym Int 64(6):773–779. https://doi.org/10.1002/pi.4851
15. Lin Z, Li L, Fu G, Lai Z, Peng A, Huang Z (2020) Molecularly imprinted polymer-based photonic crystal sensor array for the discrimination of sulfonamides. Anal Chim Acta 1101:32–40. https://doi.org/10.1016/j.aca.2019.12.032
16. Han S, Jin Y, Su L, Chu H, Zhang W (2020) A two-dimensional molecularly imprinted photonic crystal sensor for highly efficient tetracycline detection. Anal Methods 12(10):1374–1379. https://doi.org/10.1039/D0AY00110D
17. Kadhem AJ, Xiang S, Nagel S, Lin C-H, Fidalgo de Cortalezzi M (2018) Photonic molecularly imprinted polymer film for the detection of testosterone in aqueous samples. Polymers 10(4):349. https://doi.org/10.3390/polym10040349
18. Dai J, Fidalgo de Cortalezzi M (2019) Influence of pH, ionic strength and natural organic matter concentration on a MIP-fluorescent sensor for the quantification of DNT in water. Heliyon 5(6):e01922. https://doi.org/10.1016/j.heliyon.2019.e01922
19. Krishnakumar V, Balachandran V (2005) Analysis of vibrational spectra of 5-fluoro, 5-chloro and 5-bromo-cytosines based on density functional theory calculations. Spectrochim Acta Part A Mol Biomol Spectrosc 61(5):1001–1006. https://doi.org/10.1016/j.saa.2004.05.044
20. Azofra LM, Alkorta I, Elguero J (2013) Theoretical study of the mutarotation of erythrose and threose: acid catalysis. Carbohyd Res 372:1–8. https://doi.org/10.1016/j.carres.2013.01.013
21. Lin H, Wu D, Liu L, Jia D (2008) Theoretical study on molecular structures, intramolecular proton transfer reaction, and solvent effects of 1-phenyl-3-methyl-4-(6-hydro-4-amino-5-sulfo-2,3-pyrazine)-pyrazole-5-one. J Mol Struct (Thoechem) 850(1):32–37. https://doi.org/10.1016/j.theochem.2007.10.011
22. Kolar P, Classen J, Hall SG (2019) Physicochemical data of p-cresol, butyric acid, and ammonia. Data Brief 26:104356. https://doi.org/10.1016/j.dib.2019.104356
23. Zhang J, Lu T (2021) Efficient evaluation of electrostatic potential with computerized optimized code. Phys Chem Chem Phys 23(36):20323–20328. https://doi.org/10.1039/D1CP02805G
24. Jiang P, Bertone JF, Hwang KS, Colvin VL (1999) Single-crystal colloidal multilayers of controlled thickness. Chem Mater 11(8):2132–2140. https://doi.org/10.1021/cm990080+
25. Chen S, Sun H, Huang Z, Jin Z, Fang S, He J, … Lai J (2019) The visual detection of anesthetics in fish based on an inverse opal photonic crystal sensor. RSC Advances, 9(29), 16831–16838https://doi.org/10.1039/C9RA01600G
26. Zhou C, Wang T, Liu J, Guo C, Peng Y, Bai J, … Gao Z (2012) Molecularly imprinted photonic polymer as an optical sensor to detect chloramphenicol. The Analyst, 137(19), 4469https://doi.org/10.1039/c2an35617a
27. Kadhem AJ, Gentile GJ, Fidalgo de Cortalezzi MM (2021) Molecularly imprinted polymers (MIPs) in sensors for environmental and biomedical applications: a review. Molecules (Basel, Switzerland) 26(20):6233. https://doi.org/10.3390/molecules26206233
28. Nawaz T, Ahmad M, Yu J, Wang S, Wei T (2020) The biomimetic detection of progesterone by novel bifunctional group monomer based molecularly imprinted polymers prepared in UV light. New J Chem 44(17):6992–7000. https://doi.org/10.1039/C9NJ06387K
29. Nezhadali A, Es'haghi Z, Khatibi A (2016) Selective extraction of progesterone hormones from environmental and biological samples using a polypyrrole molecularly imprinted polymer and determination by gas chromatography. Analytical Methods 8(8):1813–1827. https://doi.org/10.1039/C5AY02174J11.11.008
30. Chen W, Meng Z, Xue M, Shea K (2016) Molecular imprinted photonic crystal for sensing of biomolecules. Molecular Imprinting 4:1–12. https://doi.org/10.1515/molim-2016-0001
31. Kibechu RW, Mamo MA, Msagati TAM, Sampath S, Mamba BB (2014) Synthesis and application of reduced graphene oxide and molecularly imprinted polymers composite in chemo sensor for trichloroacetic acid detection in aqueous solution. Physics and Chemistry of the Earth, Parts A/B/C 76–78:49–53. https://doi.org/10.1016/j.pce.2014.09.008
32. Huang J, Hu X, Zhang W, Zhang Y, Li G (2008) pH and ionic strength responsive photonic polymers fabricated by using

colloidal crystal templating. Colloid Polym Sci 286(1):113–118. https://doi.org/10.1007/s00396-007-1775-9
33. Kempe H, Kempe M (2010) Influence of salt ions on binding to molecularly imprinted polymers. Anal Bioanal Chem 396(4):1599–1606. https://doi.org/10.1007/s00216-009-3329-0
34. Boufas W, Dupont N, Berredjem M, Berrezag K, Becheker I, Berredjem H, Aouf N-E (2014) Synthesis and antibacterial activity of sulfonamides. SAR and DFT studies. J Mol Struct 1074:180–185. https://doi.org/10.1016/j.molstruc.2014.05.066